Accepted Manuscript

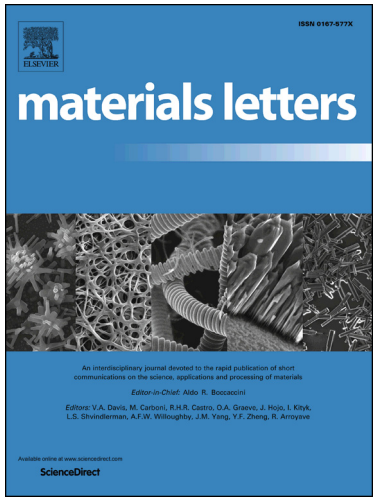

The role of phase transformation route on the intergranular corrosion susceptibility of 2205 duplex stainless steel

Nima Haghdadi, Majid Laleh, Ali Kosari, M.H. Moayed, Pavel Cizek, Peter D. Hodgson, Hossein Beladi

PII: S0167-577X(18)31914-1
DOI: https://doi.org/10.1016/j.matlet.2018.11.143
Reference: MLBLUE 25365

To appear in: *Materials Letters*

Received Date: 2 November 2018
Accepted Date: 26 November 2018

Please cite this article as: N. Haghdadi, M. Laleh, A. Kosari, M.H. Moayed, P. Cizek, P.D. Hodgson, H. Beladi, The role of phase transformation route on the intergranular corrosion susceptibility of 2205 duplex stainless steel, *Materials Letters* (2018), doi: https://doi.org/10.1016/j.matlet.2018.11.143

The role of phase transformation route on the intergranular corrosion susceptibility of 2205 duplex stainless steel

Nima Haghdadi [a,z], Majid Laleh [b], Ali Kosari [c,d], M.H. Moayed [d], Pavel Cizek [a], Peter D. Hodgson [a], Hossein Beladi [a]

[a]Deakin University, Institute for Frontier Materials, Geelong Waurn Ponds Campus, Waurn Ponds, Victoria 3216, Australia.

[b]Deakin University, School of Engineering, Faculty of Science and Technology, Geelong Waurn Ponds Campus, Waurn Ponds, Victoria 3216, Australia.

[c]Delft University of Technology, CD Delft, The Netherlands

[d]Department of Materials and Metallurgical Engineering, Ferdowsi University of Mashhad, Mashhad, Iran

[z]Correspondence to: nima.haghdadi@deakin.edu.au

ABSTRACT

Two types of austenite morphologies, equiaxed and Widmanstätten, were produced through different phase transformation routes to evaluate the critical factors affecting the intergranular corrosion susceptibility in a 2205 duplex stainless steel. These distinct austenite morphologies behaved quite differently in secondary phase precipitation on exposure to sensitization temperature. Although the Widmanstätten microstructure was found to have a larger degree of coherent ferrite/austenite interface area compared with the equiaxed one, it showed a higher degree of sensitization. It was clarified that, in addition to the ferrite/austenite interface coherency, the extent of an interface area and presence of un-stable ferrite also play prominent roles in intergranular corrosion susceptibility.

Keywords: Duplex stainless steel; Precipitation; Sensitization; Intergranular corrosion

1- INTRODUCTION

Combination of good mechanical properties together with high corrosion resistance in duplex stainless steel (DSS) makes it an attractive choice for using in marine environments, petrochemical and chemical industries [1-3]. These unique characteristics of DSSs arise from the two-phase microstructure consisting of austenite (γ) and delta ferrite (δ), which gives the opportunity to have combined properties of austenitic and ferritic stainless steels [4-6]. However, some serious problems may appear due to the microstructural changes occurring during exposure to high temperatures, associated with heat-treatment or welding [7, 8], resulting in the precipitation of different compounds such as chromium nitrides, χ-phase, σ-phase, and carbides, to list a few [9-13]. The intergranular corrosion (IGC) resistance of DSSs can be adversely influenced by the transformation and precipitation phenomena [14, 15], due to the depletion of corrosion-resistant elements in the regions adjacent to the precipitates, in the vicinity of the secondary austenite phase, and at the ferrite/austenite interface [16-18].

Although the IGC of DSSs has widely been investigated, not too much information is available regarding the influence of γ/δ interphase characteristics and the nature of microstructure on the precipitation behaviour and IGC susceptibility of 2205 DSS. It is well known that the secondary phases are more easily precipitated at an incoherent γ/δ interface than a (semi)coherent one [19, 20]. It has been clarified in our recent papers that the austenite morphology varies depending on the cooling conditions during phase transformation [21, 22], and σ-phase precipitation was shown to be dependent upon the crystallographic characteristics of γ/δ interfaces [23]. Since the precipitation of detrimental secondary phases within a certain temperature regime plays a prominent role in the IGC susceptibility of DSSs, this research aims to investigate the critical factors contributing to susceptibility to IGC in 2205 DSS with different microstructures using a double loop electrochemical potentiokinetic reactivation (DL-EPR)/microscopy analysis.

2- MATERIALS AND METHODS

A commercial 2205 DSS plate in the hot-rolled condition with a thickness of 20 mm was used as the base material in this study. Two specimens with dimensions of 10 mm × 10 mm × 20 mm were cut from the initial plate, reheated to 1370 °C in a muffle furnace in an argon atmosphere and then held at this temperature for 40 min. One specimen was slowly cooled in the furnace from 1370 °C to 970 °C with an average cooling rate of ~ 0.002 °C/s, and then immediately water-quenched from 970 °C to avoid the precipitation of any secondary phases [24]. The other specimen was directly air-cooled from 1370 °C to room temperature. Sensitization treatment was performed on the as-hot rolled, slow-cooled and air-cooled materials through reheating the specimens at 800 °C for 60 min followed by water quenching.

DL-EPR [25, 26] was used for evaluating the sensitization. Prior to the DL-EPR measurements, the specimens were first embedded in a suitable epoxy resin with an exposure area of 1 cm^2, then were ground using abrasive papers (up to 4000 grit) and finally cleaned with ethanol and dried in hot air. The DL-EPR tests were performed in 2 M H_2SO_4 + 0.5 M NaCl + 0.01 M KSCN using a saturated calomel electrode (SCE) as the reference electrode and platinum grid as the counter electrode. The tests were started by a potential sweep in the anodic direction from -0.3 V_{SCE} until the potential reached +0.3 V_{SCE} at a scanning rate of 1 mV/s. Then, the reverse scan was immediately started in the cathodic direction until the potential reached -0.3 V_{SCE}. The ratio of the current density obtained during the reactivation scan (I_r) to the current density reached during the activation scan (I_a), which is known as the degree of sensitization (DOS), gives a quantitative measure of the susceptibility of steels to intergranular corrosion generated as a result of sensitization [27-29].

The microstructure of the DSS specimens before and after sensitization treatment were characterized using scanning electron microscopy (ZEISS SUPRA 55VP FEG SEM) complemented with energy dispersive spectroscopy (EDS), and electron backscattered diffraction (EBSD) using FEI Quanta 3-D FEG SEM, both operated at 20 kV. The specimens were prepared for microstructural characterization through a standard procedure described elsewhere [23]. EBSD acquisition was performed on the RD/ND sections of the samples using a working distance of ~12 mm, a step size of 1 μm and a hexagonal grid.

3- RESULTS AND DISCUSSION

3-1- Microstructural characterization

Figure 1 (a-c) shows the microstructure of DSS specimens formed through different routes prior to the sensitization treatment revealed by the EBSD technique. The material in the as-received condition, as shown in Fig. 1a, consisted of only austenite and ferrite phases, where austenite grains (dark grey phase) embedded in the ferritic matrix (light grey phase) displayed a markedly pancaked structure as a result of the hot-rolling process (hereafter called DSS-Rolled). For the specimen slowly cooled from 1370 °C to 970 °C and then water-quenched, duplex microstructure was still conserved consisting of equiaxed austenite distributed in the matrix of delta ferrite, as presented in Fig. 1b (hereafter referred to as DSS-EQ). For the specimen air-cooled from the ferritization temperature (Fig. 1c), the microstructure consisted of large ferrite grains with Widmanstätten-like austenite particles (hereafter called DSS-Wid). During cooling, the γ-phase can form at the grain boundaries in the α-phase (known as allotriomorphic austenite), within the grains of α-phase in a plate-like manner (known as Widmanstätten side plate) and as the intergranular austenite in the α-phases In this case, the morphology of the γ-phase is acicular (needle-shaped), as shown in Fig. 1c. The microstructural

changes during these phase transformations in duplex stainless steel was discussed in detail elsewhere [22, 23]. It should be mentioned here that no other secondary precipitates were formed, except for ferrite and austenite with similar austenite/ferrite ratios during the current heat-treatment schedules. However, the phase transformation path and morphology of austenite were quite different in these specimens, which would result in different austenite/ferrite interface characteristics.

To examine the crystallographic characteristics of the interfaces, the misorientations of austenite/ferrite boundaries were investigated using EBSD (Fig. 1 d-f). Different microstructures showed differing volume fractions of coherent interfaces, i.e., those associated with the Kurdjumov–Sachs (K–S) and Nishiyama–Wassermann (N–W) orientation relationships (ORs) represented by the 42.85^0/〈0.968 0.178 0.178〉 and 45.98^0/〈0.976 0.083 0.201〉 angle/axis pairs, respectively. Considering a 2^0 deviation criterion, the overall area fractions of the austenite–ferrite interfaces corresponding to the K–S and N–W ORs were 2 and 1 % (DSS-Rolled), 12 and 4% (DSS-EQ) and 31 and 8% (DSS-Wid), respectively.

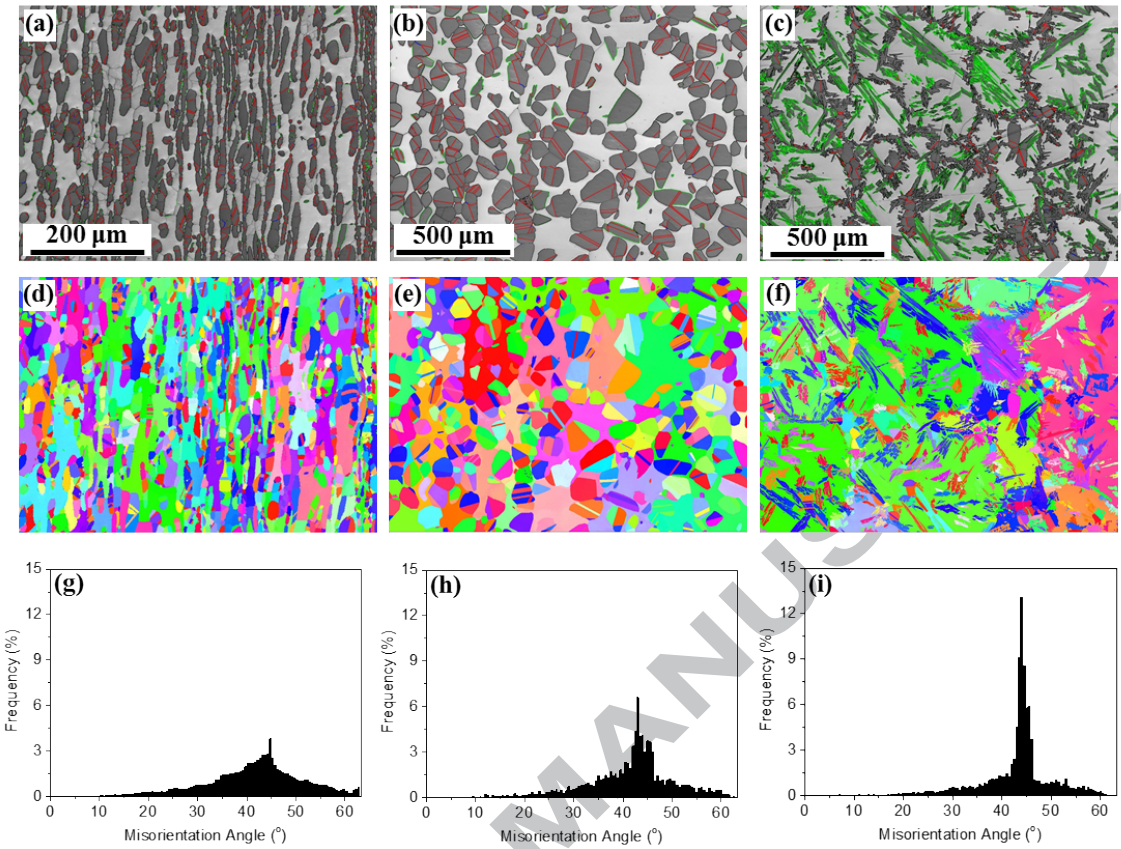

Fig 1. EBSD band contrast and IPF maps showing the microstructure of (a,d) rolled, (b,e) equiaxed and (c,f) Widmanstätten microstructures. The dark grey and light grey areas represent austenite and ferrite, respectively. The red, blue and green lines are Σ3 and Σ9 and K-S/N-W boundaries, respectively. Misorientation angle histograms for the austenite–ferrite boundaries for (g) rolled, (h) equiaxed, and (i) Widmanstätten microstructures.

Sensitized specimens in the un-etched condition were examined using the BSE mode of SEM to investigate the secondary precipitates. In SEM micrographs shown in Fig. 2, different phases can be clearly identified as γ-austenite (dark grey), δ-ferrite (darkest phase), χ-phase (brighter phase), σ-phase (light grey) and chromium-nitride (small and dark phase) [10, 30]. For DSS-Wid specimen, island-shaped secondary austenite appeared in the matrix of ferrite replete with σ-phase having a lacy morphology [31, 32]. The bright particles at the austenite/ferrite interface were identified as χ-phase by the EDS analysis. As presented in Table 1, the extent of secondary precipitates like σ-phase and chromium nitrides was higher for DSS-Wid compared with DSS-Rolled and DSS-EQ specimens, while χ-phase was higher in DSS-

Rolled followed by DSS-Wid and DSS-EQ. While a high fraction of precipitates for the rolled condition is expected based on the incoherent nature of austenite/ferrite interphases in this alloy, the higher susceptibility of DSS-Wid to precipitation compared to DSS-EQ is surprizing considering their interphases character. This can be rationalized considering the higher general population of γ-δ boundary segments (as the most important nucleation sites for precipitates) in DSS-Wid. As previously shown by the current authors [23], the content of γ-δ boundaries in DSS-Wid is more than 3 times greater than in DSS-EQ for a given area. Moreover, as the DSS-Wid has been air-cooled, it is not in its fully equilibrium state, i.e., there has not been enough time for full partitioning of alloying elements between austenite and ferrite. This might make ferrite to go through a transformation to secondary austenite, which might also be accompanied by the formation of secondary phases [33].

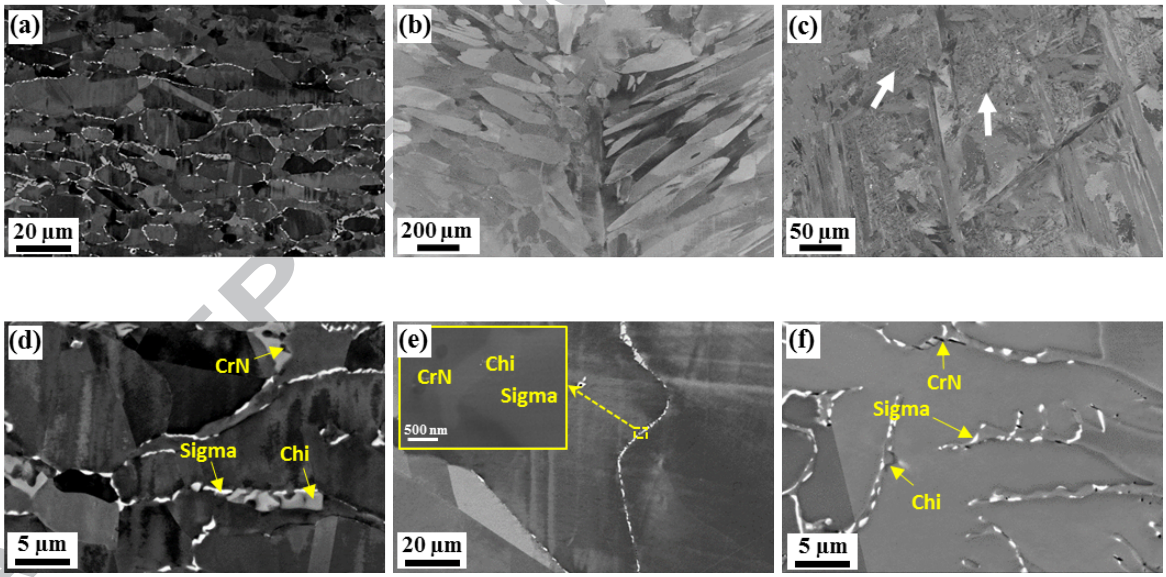

Fig 2. BSE images of the (a,d) rolled, (b,e) Equiaxed, and (c,f) Widmanstätten specimens after holding at 800 for 60 min. The white arrows in (c) show secondary austenite.

Table 1. Volume fraction of different phases formed in the microstructure after holding the samples at 800 °C for 60 min.

Area %	Rolled	Equiaxed	Widmanstätten
Sigma	6.3	3.9	6.7
Chi	1.8	0.6	1.3
Chromium Nitride	3.9	2.7	4.1
Secondary Austenite	-	-	16

3-2- IGC sensitivity

As reported widely, the secondary phases including σ, χ and Cr_2N precipitates bring about the formation of Cr-depleted regions [12, 34, 35]. The volume fraction of such phases which are highly prone to localized attack directly contributes to degree of sensitization. In this study, susceptibility of the specimens to intergranular corrosion are revealed qualitatively by oxalic acid test (Fig. 3a-f). This was studied further through collecting DL-EPR curves (Fig. 3g) by cyclic polarisation of the samples according to the procedure described in section 2. In such a measurement, the weak passivity of locally chromium-depleted regions, which are formed already in forward scanning, readily breaks down in backward scanning. Thus, the forward/backward current peak ratio is considered as a quantitative DOS criterion; the estimated values are shown in Fig. 3h.

From Fig. 3, DSS-EQ, if subjected to the sensitization process, has undergone a slight grain boundary attack. Additionally, some corrosion spots are observed within ferrite grains owing to formation of chromium-rich phases [36], but totally leading to an insignificant sensitization

as further verified by a low DOS value (~10%). Comparatively, DSS-Rolled and DSS-Wid with an identical total volume fraction of secondary phases (see Table 1) represent relatively high DOS; in their respected order, ~50% and ~60%. The slightly higher DOS of DSS-Wid, as compared to DSS-Rolled, might be attributed to the small secondary austenite particles with localized high volume of austenite-ferrite interphases that triggers sensitization [33, 37]. At this stage, it is not possible to report individual contribution of each secondary phase like σ, χ and Cr_2N to DOS; therefore, higher DOS of DSS-Wid might herein be ascribed mostly to higher intrinsic amount of interphases (see Fig. 3e and f).

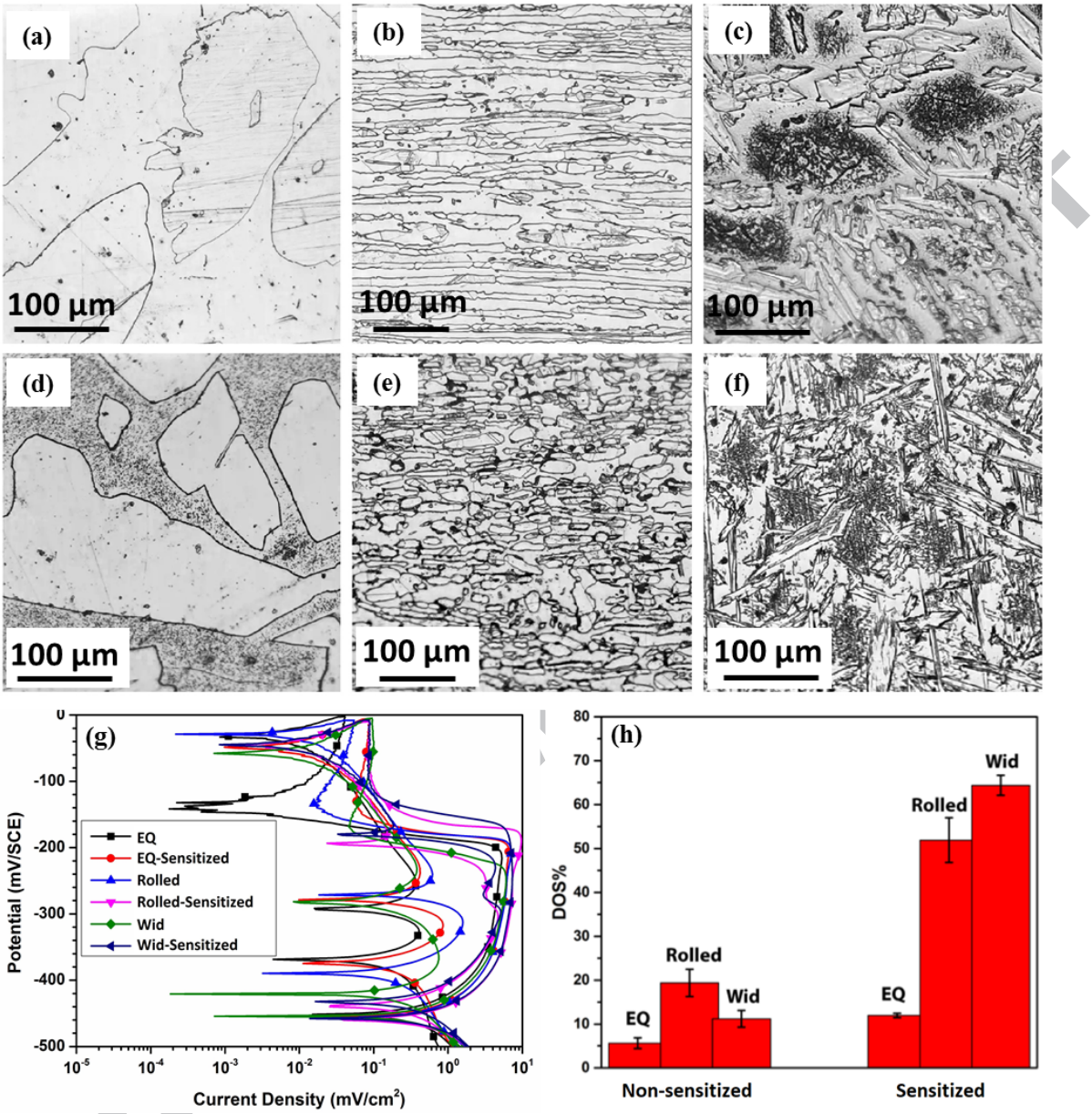

Fig 3. Corrosion-attack-morphology, revealed by an optical microscope, of non-sensitized (top row) and sensitized samples (middle row) after oxalic acid test; (a, d) Equiaxed, (b, e) Rolled and (c, f) Widmanstätten. The samples were etched electrochemically in 10% oxalic acid solution by applying 1 A/cm2 for 90 s. (g) DL-EPR curves and (h) DOS values corresponding to different sensitized and non-sensitized samples. The error bars show the standard deviation for 3 identical measurements.

4- CONCLUSIONS

The precipitation behaviour and IGC susceptibility of a 2205 DSS was investigated, revealing an evident dependence of secondary phase precipitation on the area of δ/γ interface and extent of unstable δ-phase, which in turn depended on the cooling condition during phase

transformation. Widmanstätten austenite was shown to likely form during rapid cooling rate condition and showed a larger degree of coherency at ferrite/austenite interfaces relative to the DSS-EQ. However, unexpectedly, it showed high propensity to the formation of secondary precipitates on exposure to sensitization treatment. Two factors were found to contribute to this behaviour: first, the existence of unstable δ-phase in DSS-Wid microstructure that was transformed to σ and γ_2 during sensitization treatment; second, the higher extent of interface area in the DSS-Wid compared with the DSS-EQ specimen.

ACKNOWLEDGEMENTS

The present work was carried out with the support of the Deakin Advanced Characterisation Facility. Financial support provided by the Australian Research Council is gratefully acknowledged.

REFERENCES

[1] J. Nomani, A. Pramanik, T. Hilditch, G. Littlefair, Machinability study of first generation duplex (2205), second generation duplex (2507) and austenite stainless steel during drilling process, Wear 304(1-2) (2013) 20-28.
[2] N. Ebrahimi, M.H. Moayed, A. Davoodi, Critical pitting temperature dependence of 2205 duplex stainless steel on dichromate ion concentration in chloride medium, Corrosion Science 53(4) (2011) 1278-1287.
[3] A.I. Mourad, A. Khourshid, T. Sharef, Gas tungsten arc and laser beam welding processes effects on duplex stainless steel 2205 properties, Materials Science and Engineering: A 549 (2012) 105-113.
[4] S.-M. Yang, Y.-C. Chen, C.-H. Chen, W.-P. Huang, D.-Y. Lin, Microstructural characterization of δ/γ/σ/γ2/χ phases in silver-doped 2205 duplex stainless steel under 800 C aging, Journal of Alloys and Compounds 633 (2015) 48-53.
[5] H.-Y. Liou, R.-I. Hsieh, W.-T. Tsai, Microstructure and stress corrosion cracking in simulated heat-affected zones of duplex stainless steels, Corrosion Science 44(12) (2002) 2841-2856.
[6] H. Luo, C. Dong, K. Xiao, X. Li, Characterization of passive film on 2205 duplex stainless steel in sodium thiosulphate solution, Applied surface science 258(1) (2011) 631-639.
[7] Z. Zhang, Z. Wang, Y. Jiang, H. Tan, D. Han, Y. Guo, J. Li, Effect of post-weld heat treatment on microstructure evolution and pitting corrosion behavior of UNS S31803 duplex stainless steel welds, Corrosion Science 62 (2012) 42-50.

[8] Z. Zhang, H. Jing, L. Xu, Y. Han, L. Zhao, X. Lv, J. Zhang, Influence of heat input in electron beam process on microstructure and properties of duplex stainless steel welded interface, Applied Surface Science 435 (2018) 352-366.
[9] H. Sieurin, R. Sandström, Sigma phase precipitation in duplex stainless steel 2205, Materials Science and Engineering: A 444(1-2) (2007) 271-276.
[10] N. Llorca-Isern, H. López-Luque, I. López-Jiménez, M.V. Biezma, Identification of sigma and chi phases in duplex stainless steels, Materials Characterization 112 (2016) 20-29.
[11] K.D. Ramkumar, D. Mishra, B.G. Raj, M. Vignesh, G. Thiruvengatam, S. Sudharshan, N. Arivazhagan, N. Sivashanmugam, A.M. Rabel, Effect of optimal weld parameters in the microstructure and mechanical properties of autogeneous gas tungsten arc weldments of super-duplex stainless steel UNS S32750, Materials & Design (1980-2015) 66 (2015) 356-365.
[12] S.-T. Kim, S.-H. Jang, I.-S. Lee, Y.-S. Park, Effects of solution heat-treatment and nitrogen in shielding gas on the resistance to pitting corrosion of hyper duplex stainless steel welds, Corrosion Science 53(5) (2011) 1939-1947.
[13] T. Chen, J. Yang, Effects of solution treatment and continuous cooling on σ-phase precipitation in a 2205 duplex stainless steel, Materials Science and Engineering: A 311(1-2) (2001) 28-41.
[14] F. Zanotto, V. Grassi, M. Merlin, A. Balbo, F. Zucchi, Effect of brief heat treatments performed between 650 and 850 C on corrosion behaviour of a lean duplex stainless steel, Corrosion Science 94 (2015) 38-47.
[15] S.-T. Kim, I.-S. Lee, J.-S. Kim, S.-H. Jang, Y.-S. Park, K.-T. Kim, Y.-S. Kim, Investigation of the localized corrosion associated with phase transformation of tube-to-tube sheet welds of hyper duplex stainless steel in acidified chloride environments, Corrosion Science 64 (2012) 164-173.
[16] N. Lopez, M. Cid, M. Puiggali, Influence of σ-phase on mechanical properties and corrosion resistance of duplex stainless steels, Corrosion Science 41(8) (1999) 1615-1631.
[17] C. Kwok, K. Lo, W. Chan, F. Cheng, H. Man, Effect of laser surface melting on intergranular corrosion behaviour of aged austenitic and duplex stainless steels, Corrosion science 53(4) (2011) 1581-1591.
[18] T. Takei, M. Yabe, F.-G. Wei, Effect of cooling condition on the intergranular corrosion resistance of UNS S32506 duplex stainless steel, Corrosion Science 122 (2017) 80-89.
[19] Y.S. Sato, H. Kokawa, Preferential precipitation site of sigma phase in duplex stainless steel weld metal, Scripta Materialia 40(6) (1999).
[20] Y.-J. Zhang, G. Miyamoto, K. Shinbo, T. Furuhara, Effects of α/γ orientation relationship on VC interphase precipitation in low-carbon steels, Scripta Materialia 69(1) (2013) 17-20.
[21] N. Haghdadi, P. Cizek, P. Hodgson, V. Tari, G. Rohrer, H. Beladi, Five-parameter crystallographic characteristics of the interfaces formed during ferrite to austenite transformation in a duplex stainless steel, Philosophical Magazine 98(14) (2018) 1284-1306.
[22] N. Haghdadi, P. Cizek, P. Hodgson, V. Tari, G. Rohrer, H. Beladi, Effect of ferrite-to-austenite phase transformation path on the interface crystallographic character distributions in a duplex stainless steel, Acta Materialia 145 (2018) 196-209.
[23] N. Haghdadi, D. Abou-Ras, P. Cizek, P. Hodgson, A. Rollett, H. Beladi, Austenite-ferrite interface crystallography dependence of sigma phase precipitation using the five-parameter characterization approach, Materials Letters 196 (2017) 264-268.
[24] N. Haghdadi, P. Cizek, H. Beladi, P.D. Hodgson, The austenite microstructure evolution in a duplex stainless steel subjected to hot deformation, Philosophical Magazine 97(15) (2017) 1209-1237.
[25] V.r. Čihal, R. Štefec, On the development of the electrochemical potentiokinetic method, Electrochimica Acta 46(24-25) (2001) 3867-3877.
[26] M. Laleh, F. Kargar, Suppression of chromium depletion and sensitization in austenitic stainless steel by surface mechanical attrition treatment, Materials Letters 65(12) (2011) 1935-1937.
[27] A.P. Majidi, M.A. Streicher, Potentiodynamic reactivation method for detecting sensitization in AISI 304 and 304L stainless steels, Corrosion 40(8) (1984) 393-408.

[28] A.P. Majidi, M.A. Streicher, The double loop reactivation method for detecting sensitization in AISI 304 stainless steels, Corrosion 40(11) (1984) 584-593.
[29] T. Amadou, H. Sidhom, C. Braham, Double loop electrochemical potentiokinetic reactivation test optimization in checking of duplex stainless steel intergranular corrosion susceptibility, Metallurgical and Materials Transactions A 35(11) (2004) 3499-3513.
[30] T. Chen, K. Weng, J. Yang, The effect of high-temperature exposure on the microstructural stability and toughness property in a 2205 duplex stainless steel, Materials Science and Engineering: A 338(1-2) (2002) 259-270.
[31] M. Martins, L.C. Casteletti, Heat treatment temperature influence on ASTM A890 GR 6A super duplex stainless steel microstructure, Materials characterization 55(3) (2005) 225-233.
[32] S. Ghosh, S. Mondal, High temperature ageing behaviour of a duplex stainless steel, Materials Characterization 59(12) (2008) 1776-1783.
[33] T. Chehuan, V. Dreilich, K.S. de Assis, F.V. de Sousa, O.R. Mattos, Influence of multipass pulsed gas metal arc welding on corrosion behaviour of a duplex stainless steel, Corrosion Science 86 (2014) 268-274.
[34] B. Deng, Y. Jiang, J. Xu, T. Sun, J. Gao, L. Zhang, W. Zhang, J. Li, Application of the modified electrochemical potentiodynamic reactivation method to detect susceptibility to intergranular corrosion of a newly developed lean duplex stainless steel LDX2101, Corrosion Science 52(3) (2010) 969-977.
[35] H.-J. Kim, S.-H. Jeon, S.-T. Kim, I.-S. Lee, Y.-S. Park, K.-T. Kim, Y.-S. Kim, Investigation of the sensitization and intergranular corrosion of tube-to-tubesheet welds of hyper duplex stainless steel using an electrochemical reactivation method, Corrosion Science 87 (2014) 60-70.
[36] M. Naghizadeh, M.H. Moayed, Investigation of the effect of solution annealing temperature on critical pitting temperature of 2205 duplex stainless steel by measuring pit solution chemistry, Corrosion Science 94 (2015) 179-189.
[37] V.A. Hosseini, L. Karlsson, D. Engelberg, S. Wessman, Time-temperature-precipitation and property diagrams for super duplex stainless steel weld metals, Welding in the World 62(3) (2018) 517-533.

FIGURE AND TABLE CAPTIONS

Fig 1. EBSD band contrast and IPF maps showing the microstructure of (a,d) rolled, (b,e) equiaxed and (c,f) Widmanstätten microstructures. The dark grey and light grey areas represent austenite and ferrite, respectively. The red, blue and green lines are Σ3 and Σ9 and K-S/N-W boundaries, respectively. Misorientation angle histograms for the austenite–ferrite boundaries for (g) rolled, (h) equiaxed, and (i) Widmanstätten microstructures.

Fig 2. BSE images of the (a,d) rolled, (b,e) Equiaxed, and (c,f) Widmanstätten specimens after holding at 800 for 60 min. The white arrows in (c) show secondary austenite.

Fig 3. Corrosion-attack-morphology, revealed by an optical microscope, of non-sensitized (top row) and sensitized samples (middle row) after oxalic acid test; (a, d) Equiaxed, (b, e) Rolled and (c, f) Widmanstätten. The samples were etched electrochemically in 10% oxalic acid solution by applying 1 A/cm^2 for 90 s. (g) DL-EPR curves and (h) DOS values corresponding to different sensitized and non-sensitized samples. The error bars show the standard deviation for 3 identical measurements.

Table 1. Volume fraction of different phases formed in the microstructure after holding the samples at 800 °C for 60 min.

HIGHLIGHTS

- Two types of austenite morphologies, equiaxed (EQ) and Widmanstätten (W), were produced.
- W-A showed a larger degree of coherency at δ/γ interfaces relative to the EQ-A.
- W-A showed unexpected propensity to the formation of secondary precipitates.
- Higher extent of interface area and unstable δ were found to contribute to this behaviour.